Journal of Reproduction and Development, Vol. 64, No 2, 2018

—Original Article—

Peroxiredoxin as a functional endogenous antioxidant enzyme in pronuclei of mouse zygotes

Kohtaro MORITA[1)], Mikiko TOKORO[2)], Yuki HATANAKA[3, 4)], Chika HIGUCHI[1)], Haruka IKEGAMI[1)], Kouhei NAGAI[1)], Masayuki ANZAI[1, 5)], Hiromi KATO[1, 5)], Tasuku MITANI[1, 5)], Yoshitomo TAGUCHI[1)], Kazuo YAMAGATA[1)], Yoshihiko HOSOI[1)], Kei MIYAMOTO[1)] and Kazuya MATSUMOTO[1)]

[1)]*Laboratory of Molecular Developmental Biology, Graduate School of Biology-Oriented Science and Technology, Kindai University, Wakayama 649-6493, Japan*
[2)]*The Asada Institute for Reproductive Medicine, Asada Ladies Clinic, Kasugai, Aichi 486-0931, Japan*
[3)]*RIKEN BioResource Center, Ibaraki 305-0074, Japan*
[4)]*Medical Research Council Clinical Sciences Centre, Imperial College London, London W12 0NN, UK.*
[5)]*Institute of Advanced Technology, Kindai University, Wakayama 642-0017, Japan*

Abstract. Antioxidant mechanisms to adequately moderate levels of endogenous reactive oxygen species (ROS) are important for oocytes and embryos to obtain and maintain developmental competence, respectively. Immediately after fertilization, ROS levels in zygotes are elevated but the antioxidant mechanisms during the maternal-to-zygotic transition (MZT) are not well understood. First, we identified peroxiredoxin 1 (PRDX1) and PRDX2 by proteomics analysis as two of the most abundant endogenous antioxidant enzymes eliminating hydrogen peroxide (H_2O_2). We here report the cellular localization of hyperoxidized PRDX and its involvement in the antioxidant mechanisms of freshly fertilized oocytes. Treatment of zygotes at the pronuclear stage with H_2O_2 enhanced pronuclear localization of hyperoxidized PRDX in zygotes and concurrently impaired the generation of 5-hydroxymethylcytosine (5hmC) on the male genome, which is an epigenetic reprogramming event that occurs at the pronuclear stage. Thus, our results suggest that endogenous PRDX is involved in antioxidant mechanisms and epigenetic reprogramming during MZT.

Key words: Hydrogen peroxide (H_2O_2), Mouse, Peroxiredoxin (PRDX), Zygotes

(**J. Reprod. Dev. 64:** 161–171, 2018)

Oocytes within follicles and those in the oviduct are exposed to reactive oxygen species (ROS) [1]. These moderate amounts of ROS are involved not only in various cellular signaling but also in cell cycles such as diplotene arrest, resumption, and metaphase II (MII) arrest in oocytes [1–3]. However, in the case of excessive ROS production, oxidative stress causes mitochondrial alterations, perturbed embryonic development, ATP depletion, apoptosis, and fragmentation [4, 5]. To prevent excessive accumulation of ROS in normal oocytes and embryos, various antioxidant enzymes are generally involved in controlling the ROS level [4, 5]. As a mechanism of eliminating intracellular ROS, superoxide, arising from oxygen metabolism in mitochondria, is converted to hydrogen peroxide (H_2O_2) by superoxide dismutase (SOD) and H_2O_2 is promptly eliminated by glutathione (GSH) which is catalyzed by some antioxidant enzymes such as glutathione peroxidase (GPX) [4–8]. The function of GSH as the most abundant endogenous reducer in animal cells has been demonstrated in mouse oocytes and embryos [4–8]. In fact, mice deficient in GSH synthesis die before E8.5, hence GSH is required for embryo development [9]. In addition to GSH, thioredoxin (TRX) is another redox protein widely preserved in various organisms, from archaea and bacteria to humans [10]. TRX plays a role in the maintenance of antioxidant enzymes that directly eliminate H_2O_2 by reducing oxidized enzymes [10]. TRX knockout mice are embryonic lethal around E10.5 [11]. In these ways, the GSH and TRX systems regulate the ROS levels in early embryos as well as cultured cells [4–11].

While ovulated oocytes are protected from ROS and are maintained in the intracellular redox state by antioxidant enzymes [4, 5], ROS levels increase in zygotes immediately after fertilization [12, 13]. Indeed, various important phenomena occur in freshly fertilized oocytes, including Ca^{2+} oscillations, meiosis resumption, 2nd polar body extrusion, protamine-histone exchange, DNA demethylation on the male genome, and DNA replication [14, 15]. In the case of excessive H_2O_2-treatment of pronuclear-formed zygotes, DNA damage increases and cleavage is arrested [16, 17]. Although it seems to be important for adequately maintaining ROS levels in fertilized oocytes as well as ovulated oocytes, the antioxidant mechanism of endogenous proteins in freshly fertilized oocytes has not been well understood.

In this study, we explored abundant the antioxidant enzymes using

Received: January 7, 2018
Accepted: January 19, 2018
Published online in J-STAGE: March 2, 2018

Correspondence: K Matsumoto (e-mail: kazum@waka.kindai.ac.jp)

mouse zygotes by proteomics analysis to uncover the antioxidant mechanisms in zygotes. As a result, peroxiredoxin 1 (PRDX1) was identified as the most abundant antioxidant enzyme in zygotes. PRDX proteins play a role of catalyzing the reduction of cellular hydrogen peroxide (H_2O_2) to H_2O in the TRX/PRDX system [18]. Interestingly, immunocytochemical analysis showed that hyperoxidized PRDX family members including PRDX1 were localized in the male and female pronuclei of zygotes. Hyperoxidized PRDX proteins in the pronuclei of H_2O_2-treated zygotes at PN3 were significantly increased compared to those in untreated controls. Concurrently, 5-hydroxymethylcytosine (5hmC) was significantly decreased in the male pronuclei of zygotes. Thus, our results indicate the necessity to investigate the relationship between antioxidant enzymes and epigenetic reprogramming in further research.

Materials and Methods

Animals

All mice (ICR strain) were purchased from Kiwa Laboratory Animals (Wakayama, Japan) and maintained in light-controlled, air-conditioned rooms. This study was carried out in strict accordance with the recommendations in the Guidelines of Kindai University for the Care and Use of Laboratory Animals. Experimental protocols were approved by the Committee on the Ethics of Animal experiments of Kindai University (Permit Number: KABT-26-002). All mice were killed by cervical dislocation and all efforts were made to minimize suffering and to reduce the number of animals used in the present study.

In vitro fertilization and embryo culture

Collection of spermatozoa, oocytes, and zygotes were performed as described in previous studies [19–25]. Spermatozoa were collected from the cauda epididymidis of male mice. The sperm suspension was incubated in human tubal fluid (HTF) medium for 1.5 h to allow for capacitation at 37°C under 5% CO_2 in air. Oocytes were collected from the excised oviducts of female mice (2–3 months old) that were superovulated with pregnant mare serum gonadotropin (PMSG; Serotropin, Teikoku Zoki, Tokyo, Japan) and 48 h later, human chorionic gonadotropin (hCG; Puberogen, Sankyo, Tokyo, Japan). Cumulus-oocyte complexes were recovered into pre-equilibrated HTF medium. The sperm suspension was added to the oocyte cultures and morphologically normal zygotes were collected 2 h after insemination. The zygotes were cultured in potassium simplex optimized medium (KSOM) [26] at 37°C under 5% CO_2 in air.

Two-dimensional gel electrophoresis (2-DE)

600, 10,000, and 15,000 MII oocytes for obtaining 2-DE master gels, and 600 MII oocytes and 600 zygotes for obtaining the gels for quantitative analysis of protein spots, in each case were sonicated three times at 4°C for 30 sec. The sonicated samples were resuspended in lysis buffer composed of 7 M urea, 2 M thiourea, 4% CHAPS, 0.5% immobilized pH gradient (IPG) buffer (GE Healthcare, Little Chalfont, UK), 0.05% tri-n-butylphosphine, 1 tablet per 10 ml complete mini protease inhibitor (Roche, Mannheim, Germany), and traces of bromophenol blue (BPB). The resuspended samples were precipitated with three volumes of 100% acetone and mixed with rehydration solution (7 M urea, 2 M thiourea, 4% CHAPS, 0.05% tri-n-butylphosphine, IPG buffer, and traces of BPB). The 2-DE procedure was performed as described previously [27, 28]. The obtained proteins were separated in the first dimension on immobilized pH gradient IPG gels (Immobiline DryStrip, pH 3-11 nonlinear gradient, 13 cm, GE Healthcare). IPG gels were rehydrated overnight with rehydration solution containing protein samples. First-dimension electrophoresis was performed at 15°C under the following conditions: 1 min of linear gradient from 0 to 500 V, 8 h of constant voltage at 500 V, 1.5 h of linear gradient from 500 to 3,500 V, and 5.4 h of constant voltage at 3,500 V. Strips were then washed with distilled water and equilibrated at RT for 15 min in 5 ml of equilibration buffer composed of 6 M urea, 50 mM Tris-HCl (pH 8.0), 30% glycerol, 2% SDS, 50 mg DTT, and traces of BPB before being incubated for 15 min in an equilibration solution of the same composition except for 125 mg iodoacetamide replacing the DTT. The equilibrated strips were transferred onto the SDS-PAGE gel. Second dimension electrophoresis was performed on 12% polyacrylamide gels in CoolPhoreStar SDS-PAGE Tetra-200 (Anatech, Tokyo, Japan) with a constant current of 30 mA per gel for 1 h.

Visualization and image analysis of 2-DE gels

The gels were fixed with a fixation solution containing 10% methanol and 7% acetic acid for 30 min at room temperature (RT) and then transferred to distilled water for 20 min. The gels were stained with SYPRO Ruby (Invitrogen, Carlsbad, CA, USA) overnight and then washed with 10% ethanol. Gel images were obtained using an AlphaImager (Alpha Innotech, San Leandro, CA, USA) and analyzed using Progenesis PG220 and TT900 (Nonlinear Dynamics, Newcastle upon Tyne, UK) for spot detection, quantification, and comparative analysis.

MALDI sample preparation

For protein identification by mass spectrometry, protein spots in the 2-DE master gels from each 600, 10,000, and 15,000 MII oocytes were collected by gloved hand on a Safe Imager blue light transilluminator (Invitrogen). Gel pieces were incubated three times in destaining solution consisting of 50% acetonitrile (ACN) in 50 mM ammonium bicarbonate for 20 min at 37°C. The gel pieces were then incubated in 100% ACN for 1 min before being dried completely. The obtained proteins were digested with 1.67 µg/ml trypsin (Promega, Southampton, UK) in 25 mM ammonium bicarbonate at 30°C overnight. The digested proteins were purified and concentrated using ZipTipTMµC18 (Millipore, Bedford, MA, USA). The peptides absorbed in the gel were directly eluted onto the MALDI sample plate using 2.5 mg/ml α-cyano-4-hydroxycinnamic acid (Waters, Milford, MA, USA) in 70% ACN containing 0.1% trifluoroacetic acid.

MALDI-TOF/MS

MS spectrometric analysis of the tryptic was performed using a 4700 MALDI-TOF/TOF mass spectrometer (Applied Biosystems, Foster City, CA, USA). MS spectra were measured in the positive-ion reflector mode with a mass range from 700 to 3,500. Data were subjected to external calibration with five standard peptides (Sigma, St. Louis, MO, USA). The MS/MS spectra were measured in CID

mode. From a single parent MS spectrum, the five most abundant ions were selected for MS/MS analysis. The data were subjected to external calibration using fragment peaks of the human ACTH peptide 18-39 (MH1 2465. 1989, Sigma). The raw MS and MS/MS data were used in database searches using the MASCOT search engine (Matrix Science, London, UK, http://www.matrixscience.com/) and UniProt (http://www.uniprot.org/) with a mass tolerance of 0.2 Da.

Western blot analysis

Western blotting was performed as described previously [19–21, 23–25, 28, 29]. Samples (30 MII oocytes or zygotes for PRDX1 detection and 50 MII oocytes or zygotes for PRDX-$SO_{2/3}$ detection) were subjected to sodium dodecyl sulfate (SDS) polyacrylamide gel electrophoresis. Each sample was treated with the same volume of 2 × SDS sample buffer (125 mM Tris-HCl (pH 6.8), 4% SDS, 0.02% BPB, 20% glycerol, and 10% 2-mercaptoethanol) before SDS-PAGE. Non-reduced samples were prepared without the 10% 2-mercaptoethanol [30]. Proteins were resolved in 12% running gels for 2 h and electrophoretically transferred to polyvinylidene difluoride (PVDF) membranes (GE Healthcare) for 1.5 h. The membrane was washed with phosphate-buffered saline (PBS), incubated in Block Ace (Dainippon-Pharm, Osaka, Japan) at RT for 1 h, washed twice with PBS containing 0.2% Tween 20 (PBST) for 10 min, and incubated at 4°C overnight with anti-PRDX1 antibody (1:100,000; Abcam, Cambridge, UK; ab41906), anti-PRDX-$SO_{2/3}$ antibody (1:2,000; Abcam; ab16830), and anti-Actin antibody (1:10,000; Sigma; A5441) as a loading control. The membrane was washed in PBST, incubated with donkey anti-rabbit IgG-horseradish peroxidase (HRP) conjugate (1:200,000; Sigma; A0545) and donkey anti-goat IgG HRP conjugate (1:200,000; Millipore; AP180P) at RT for 1 h, washed three times with PBST for 10 min, and developed using ECL Prime Western Blotting detection reagent (GE Healthcare).

Immunocytochemistry of zygotes

The classification of pronuclear (PN) stages was performed according to previous studies [31], where the pronuclear morphology and hours post-insemination (hpi) were taken into consideration. The subcellular localization of PRDX1, PRDX-$SO_{2/3}$, 5-methylcytosine (5mC), and 5hmC was determined by immunocytochemical analysis of zygotes, as described [19–22, 24, 25, 32]. Embryos were fixed in 10% formaldehyde neutral buffer solution (Nakalai Tesque, Kyoto, Japan) at RT for 15 min and the zona pellucida was removed with acid Tyrode's solution. Samples were then washed three times in PBS containing 3% bovine serum albumin (PBS-BSA) and permeabilized with PBS-BSA containing 0.5% Triton X-100 (Nakalai Tesque) at RT for 15 min. For 5mC and 5hmC, the specimens were denatured with 4 N HCl at RT for 10 min and then neutralized with 40 mM Tris-HCl (pH 8.5) for 20 min. They were then incubated with anti-PRDX1 antibody (1:20,000), anti-PRDX-$SO_{2/3}$ antibody (1:2,000; Abcam; ab16830), anti-5mC antibody (1:2,000; Calbiochem, Darmstadt, Germany; NA81), or anti-5hmC antibody (1:2,000; Active motif, Carlsbad, CA, USA; 39769) in PBS-BSA at 4°C overnight. After incubation, the samples were treated with Alexa Fluor 555-labeled donkey anti-rabbit IgG secondary antibody (1:2,000; Life Technologies, Carlsbad, CA, USA; A-21207) for anti-PRDX1, PRDX-$SO_{2/3}$, and 5hmC antibodies, with an Alexa Fluor 488-labeled donkey anti-mouse IgG secondary antibody (1:2,000; Invitrogen; A21202) for detection of the 5mC antibody, all at RT for 1 h. PRDX1-, PRDX-$SO_{2/3}$-, 5mC- and 5hmC-stained zygotes were each mounted into VECTASHIELD (Vector Laboratories, Burlingame, CA, USA) mounted on the slide glasses containing 3 μg/ml 4′ 6-diamidino-2-phenylindole (DAPI) (Invitrogen; D1306). Finally, the PRDX1-, PRDX-$SO_{2/3}$-stained zygotes were imaged using a conventional upright microscope (Axioplan2, Carl Zeiss, Jene, Germany) equipped with a mercury lamp (HBO 100, Carl Zeiss), and digital CCD camera (AxioCamMRc5, Carl Zeiss). The 5mC-, 5hmC-, and PRDX-$SO_{2/3}$-stained zygotes were imaged using a confocal laser-scanning microscope (LSM 800, Carl Zeiss) equipped with 40 × and 63 × silicon oil-immersion objectives (Carl Zeiss).

Immunocytochemistry of cumulus cells

Cumulus cells obtained by *in vitro* fertilization were fixed in 4% PFA at RT for 15 min. Those cells were permeabilized with PBS-BSA containing 0.5% Triton X-100 at RT for 15 min and then incubated with anti-PRDX-$SO_{2/3}$ antibody (1:2,000) in PBS-BSA at 4°C overnight. After incubation, the cells were treated with an Alexa Fluor 555 labeled donkey anti-rabbit IgG secondary antibody (1:2,000) for anti-PRDX-$SO_{2/3}$ at RT for 1 h. Specimens were mounted on glass slides in VECTASHIELD mounting medium containing 3 μg/ml DAPI. Finally, the slides were imaged using a confocal laser-scanning microscope (LSM 800, Carl Zeiss) equipped with a 63 × silicon oil-immersion objective (Carl Zeiss).

Treatment of mouse zygotes with H_2O_2

Previously, it was shown that mouse zygotes treated with 200 μM H_2O_2 for 15 min results in the inhibition of cleavage and/or fragmentation [17]. To induce oxidative stress in early mouse zygotes, freshly fertilized oocytes at 1 hpi were incubated in KSOM including 10, 50, 100 or 200 μM H_2O_2 at 37°C under 5% CO_2 in air for 5 h. For the control, the same protocol was used without H_2O_2. At 6 hpi, fertilized oocytes were washed with KSOM prior to further analysis. Preliminarily we determined the H_2O_2 concentration that did not affect embryonic survival and pronuclei formation in freshly fertilized oocytes at 6 hpi, which is approximately PN3 [31]. As shown in Supplementary Table 1 (online only), the zygotes were able to form pronuclei in 100 μM H_2O_2-treatment at least until 6 hpi and maintained developmental ability to the 2-cell stage. In this study, we used 100 μM H_2O_2 as an optimal oxidative stress condition.

Statistical analysis

For statistical analysis, we used StatView version 5.0 (SAS Institute, Cary, NC, USA) and performed the analysis of Chi-square distribution and nonparametric test (Mann-Whitney U test) with an α level of 0.05 to determine possible statistically significant differences.

Results

Identification of endogenous antioxidant enzymes that are abundantly present in mouse MII oocytes and zygotes

We tried to explore the most abundant antioxidant enzymes in mouse zygotes in order to investigate the mechanisms of reducing ROS. However, it is more demanding to collect a large number of

zygotes for proteomics analysis than to collect MII oocytes. Here, we decided to use MII oocytes instead of zygotes for proteomic analysis because zygotic genome activation (ZGA) occurs from the late 1-cell to early 2-cell stages and maternal proteins are stored in oocytes until ZGA [33, 34]. First, we performed 2-DE using MII oocytes, and obtained the 2-DE gel photos (Fig. 1 A). Next, we analyzed the 2-DE gel photos to construct a reference gel for comparing the protein spots (Fig. 1A). As a result, 449 protein spots were commonly detected on the gels in the 3 to 11 pH range and 10–200 kDa range (Fig. 1A), and 137 protein spots (64 protein species) were identified from these gels by MALDI-TOF/MS (Supplementary Table 2: online only). Furthermore, we examined changes in protein expression from MII oocytes to zygotes by comparing the 2-DE gels from 600 MII oocytes and 600 zygotes (Fig. 1B). PRDX1 and PRDX2 were identified as the TRX system in MII oocytes and zygotes, and the expression levels of all identified proteins were hardly changed between the MII oocytes and the zygotes (Table 1 and Supplementary Table 3: online only). We detected PRDX1 and PRDX2 as the ninth and twenty-second highest expressing proteins, respectively, among the 64 proteins identified in the mouse zygotes (Table 1). PRDX family members (PRDX1-4), which are mainly reduced by TRX, eliminate H_2O_2 in various cellular locations [35–38], we focused on not only PRDX1 but also the function of all PRDX family members as reducers in this study.

Existence of oxidized PRDX1 in the pronuclei of zygotes

To reveal the localization of PRDX1, we performed immunocytochemical analysis. PRDX1 signals were observed both in the cytoplasm and pronuclei of zygotes at PN5, although the signals were mostly observed in the cytoplasm at PN1-4 (Fig. 2A). PRDX family proteins contain an N-terminal Cys that is selectively oxidized as a substitute for other proteins, and oxidized PRDX1-4 have a characteristic to form homodimers mediated by a disulfide bond [35–38]. To examine whether PRDX1 acts as a reducer during pronuclear stages, we attempted to distinguish dimeric PRDX1 using non-reducing SDS-PAGE conditions which leave disulfide bonds intact [30, 39]. As a result, we detected PRDX1 signals at approximately 44 kDa, equivalent to the dimeric form, and no PRDX1 signals at approximately 22 kDa, equivalent to the monomeric form (Fig. 2B). These results indicate that PRDX1 is oxidized during the pronuclear stages of zygotes.

Hyperoxidation of PRDX family members in pronuclear zygotes

PRDX family members, including PRDX1, are hyperoxidized by excessive H_2O_2 before being reduced by TRX [35–38]. To investigate the profile of hyperoxidized PRDX family members in zygotes, we performed immunocytochemical and immunoblot analyses using anti-PRDX-$SO_{2/3}$ antibody, which recognizes the hyperoxidized form of PRDX family members (PRDX1-4). Interestingly, the PRDX-$SO_{2/3}$ signals were observed intensely in pronuclei throughout PN2-5 (Fig. 3A), although pronuclear PRDX1 signals were clearly observed only at PN5 (Fig. 2A). Furthermore, hyperoxidized PRDX was detected as the dimeric form during pronuclear stages (Fig. 3B). Our findings suggest that the other PRDX family members in addition to PRDX1 may play key roles as reducers in the pronuclei and cytoplasm of zygotes.

Next, to test whether the pronuclear accumulation of hyperoxidized PRDX is specific to zygotes compared with somatic cells, we performed immunocytochemical analysis using anti-PRDX- $SO_{2/3}$ antibody in cumulus cells, which seem to be exposed to exogenous oxidative stress under the same condition as zygotes. PRDX-$SO_{2/3}$ signals were not observed in the nuclei of cumulus cells (Fig. 3C). Taken together, these results suggest the possibility of specific functions of PRDX family members as endogenous antioxidant enzymes in pronuclei of zygotes.

Accumulation of hyperoxidized PRDX in pronuclei of H_2O_2-treated zygotes and the dynamics of 5hmC in male pronuclei of H_2O_2-treated zygotes

Since one of the specific events occurring in the pronuclei of zygotes is active DNA demethylation of the male pronucleus [40, 41], the possibility of zygotic-specific functions of pronuclear PRDX family members led us to examine the involvement of PRDX in active DNA demethylation of the male pronuclei of zygotes. To address this under oxidative stress conditions by H_2O_2-treatment, we performed localization assays using antibodies to 5mC, 5hmC, and PRDX-$SO_{2/3}$ in freshly fertilized oocytes at 6 hpi (Fig. 4A), which corresponds to approximately PN3 [31]. A large amount of PRDX-$SO_{2/3}$ was significantly observed in the male and female pronuclei of H_2O_2-treated zygotes compared to those of untreated ones (male pronucleus: $P = 0.0038$, female pronucleus: $P = 0.0020$), although PRDX-$SO_{2/3}$ was clearly present in the pronuclei and cytoplasm of both treated and untreated zygotes (Fig. 4B, 4C, and Supplementary Fig. 1A: online only). The observation that hyperoxidized PRDX predominantly accumulated in the pronuclei of zygotes was confirmed under the oxidative damage conditions induced by H_2O_2 treatment, indicating that the PRDX functions as endogenous antioxidant enzymes in the pronuclei of zygotes. Next, we found that there was a significant decrease in the level of 5hmC in male pronuclei of H_2O_2-treated zygotes ($P = 0.002$; Fig. 4D, 4F, and Supplementary Fig. 1B), indicating that the accumulation of hyperoxidized PRDX in the male pronuclei of zygotes correlates with a decrease in the observed amount of 5hmC, an oxidation product of 5mC by Tet methylcytosine dioxygenase 3 (Tet3). These results collectively suggest that endogenous PRDX is involved in both the antioxidant mechanisms and epigenetic reprogramming of freshly fertilized oocytes.

Discussion

In this study, we identified PRDX1 and PRDX2 as abundantly expressed endogenous antioxidants in MII oocytes and zygotes (Table 1 and Supplementary Table 3). Moreover, we also identified 9 reductases, which catalyze NAD (P) $^+$ to NAD (P) H, and glutathione S-transferase A4 (GSTA4) as the GSH system, although these proteins do not directly reduce ROS (Table 1 and Supplementary Table 2). In total, 12 redox proteins (19% of the identified 64 proteins) were abundantly expressed in MII oocytes and zygotes (Table 1 and Supplementary Table 3). In a previous proteomics analysis, 7,349 proteins were identified from 28 mouse tissues, and various antioxidants such as the TRX system, GSH system, and SOD are

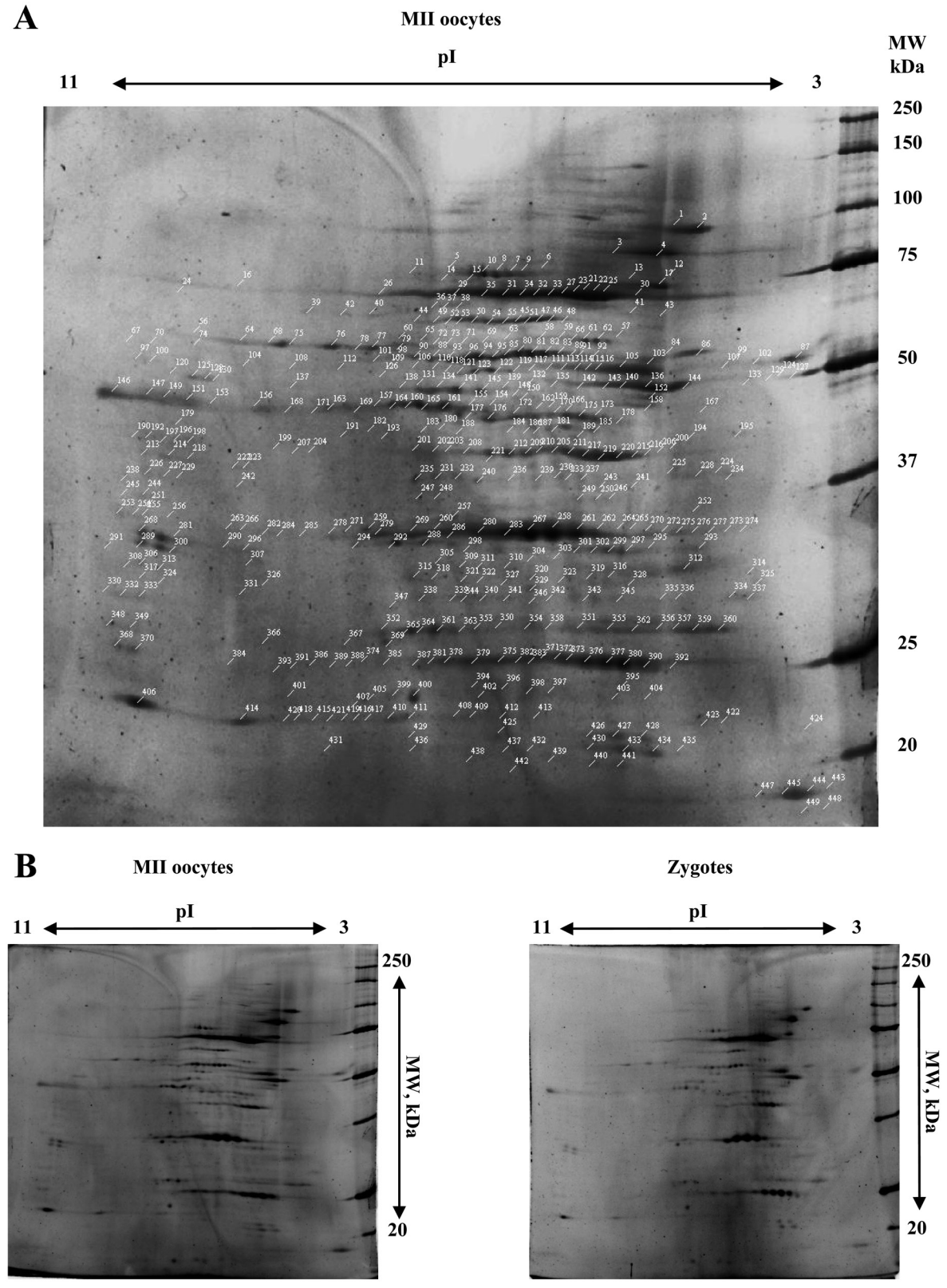

Fig. 1. Proteins from mouse oocytes and zygotes as separated by 2-DE. (A) Representative 2-DE master gel from 600 MII oocytes. (B) Representative 2-DE gels from 600 MII oocytes and 600 zygotes. The original gel size was 16 × 16 × 0.1 cm. MW, molecular weight; pI: isoelectric point.

Table 1. The ranking of identified protein expression levels in mouse zygotes

Ranking	Protein names	Accesion No.	Entry name	Quantity
1	L-lactate dehydrogenase B chain	P16125	LDHB_MOUSE	14.61349669
2	Protein-arginine deiminase type-6	Q8K3V4	PADI6_MOUSE	9.947769597
3	Ubiquitin carboxyl-terminal hydrolase isozyme L1	Q9R0P9	UCHL1_MOUSE	7.702796872
4	Actin, cytoplasmic 1	P60710	ACTB_MOUSE	3.48404797
5	Tubulin beta-4B chain	P68372	TBB4B_MOUSE	3.392538556
6	Heat shock protein HSP 90-alpha	P07901	HS90A_MOUSE	3.348318752
7	Tubulin alpha-1C chain	Q52L87	Q52L87_MOUSE	2.62285433
8	KH domain-containing protein 3	Q9CWU5	Q9CWU5_MOUSE	1.894142208
9	Peroxiredoxin-1	P35700	PRDX1_MOUSE	1.529494804
10	Eukaryotic initiation factor 4A-I	P60843	IF4A1_MOUSE	1.206222115
11	S-phase kinase-associated protein 1	Q9WTX5	SKP1_MOUSE	1.082481973
12	14-3-3 protein zeta/delta	P63101	1433Z_MOUSE	1.068961564
13	Endoplasmin	P08113	ENPL_MOUSE	1.042286339
14	ATP synthase subunit beta, mitochondrial	P56480	ATPB_MOUSE	0.995851569
15	Nucleoplasmin-2	Q80W85	NPM2_MOUSE	0.95406047
16	Protein disulfide-isomerase A3	P27773	PDIA3_MOUSE	0.895400314
17	78 kDa glucose-regulated protein	P20029	GRP78_MOUSE	0.811152719
18	Glucose-6-phosphate 1-dehydrogenase X	Q00612	G6PD1_MOUSE	0.790972039
19	Protein disulfide-isomerase	P09103	PDIA1_MOUSE	0.734501192
20	Putative uncharacterized protein	Q3TAQ8	Q3TAQ8_MOUSE	0.733769625
21	Putative uncharacterized protein	Q3TLF7	Q3TLF7_MOUSE	0.732392466
22	Peroxiredoxin-2	Q61171	PRDX2_MOUSE	0.625146201
23	Radixin	Q3TS85	RADI_MOUSE	0.598707237
24	60 kDa heat shock protein, mitochondrial	P63038	CH60_MOUSE	0.57122068
25	Aldose reductase	P45376	ALDR_MOUSE	0.53744403
26	Pyruvate kinase PKM	P52480	KPYM_MOUSE	0.534408468
27	Creatine kinase B-type	Q04447	KCRB_MOUSE	0.444933384
28	Zinc finger BED domain-containing protein 3	Q9D0L1	ZBED3_MOUSE	0.430290485
29	Phosphatidylethanolamine-binding protein 1	P70296	PEBP1_MOUSE	0.414322341
30	Putative uncharacterized protein	Q3U939	Q3U939_MOUSE	0.354005009
31	Egg and early embryo abundant protein	Q64GA5	Q64GA5_MOUSE	0.290313318
32	Annexin A7	Q3TT33	ANXA7_MOUSE	0.289730038
33	PREDICTED: similar to Glyceraldehyde-3-phosphate dehydrogenase (GAPDH)	XP_001480200	-	0.278729149
34	Prohibitin	P67778	PHB_MOUSE	0.278628484
35	Putative uncharacterized protein	Q9CRT0	Q9CRT0_MOUSE	0.273911203
36	Dihydrolipoyl dehydrogenase, mitochondrial	O08749	DLDH_MOUSE	0.246744539
37	Pla2g4c protein	Q7TN01	Q7TN01_MOUSE	0.232697789
38	Elongation factor 1-alpha 1	P10126	EF1A1_MOUSE	0.212137263
39	Putative uncharacterized protein	Q8BPH1	Q8BPH1_MOUSE	0.209307486
40	Putative uncharacterized protein	Q3UYL0	Q3UYL0_MOUSE	0.207188221
41	Translationally-controlled tumor protein	P63028	TCTP_MOUSE	0.206617326
42	Glutathione S-transferase A4	P24472	GSTA4_MOUSE	0.205718817
43	Putative uncharacterized protein	Q3U9J7	Q3U9J7_MOUSE	0.182901269
44	PREDICTED: similar to Glyceraldehyde-3-phosphate dehydrogenase (GAPDH) isoform 1	XP_001474783	-	0.182027629
45	40S ribosomal protein SA	P14206	RSSA_MOUSE	0.177655517
46	Gamma-glutamylcyclotransferase	Q9D7X8	GGCT_MOUSE	0.163073478
47	ADP-sugar pyrophosphatase	Q9JKX6	NUDT5_MOUSE	0.158428081
48	Aldehyde dehydrogenase, mitochondrial	P47738	ALDH2_MOUSE	0.133313632
49	Peroxisomal trans-2-enoyl-CoA reductase	Q99MZ7	PECR_MOUSE	0.130433536
50	Ubiquitin thioesterase OTUB1	Q7TQI3	OTUB1_MOUSE	0.103403201
51	COP9 signalosome complex subunit 7a	Q9CZ04	CSN7A_MOUSE	0.094011629
52	Alcohol dehydrogenase [NADP+]	Q9JII6	AK1A1_MOUSE	0.090318867
53	ATP synthase subunit alpha, mitochondrial	Q03265	ATPA_MOUSE	0.072855814
54	Glucosamine-6-phosphate isomerase 2	Q9CRC9	GNPI2_MOUSE	0.063006543
55	Spindlin-1	Q61142	SPIN1_MOUSE	0.059002231
56	Actin, cytoplasmic 2	P63260	ACTG_MOUSE	0.0572195
57	PREDICTED: similar to Phosphatidylethanolamine-binding protein	XP_921327	-	0.052495976
58	Protein EFR3 homolog B	Q6ZQ18	EFR3B_MOUSE	0.042847602
59	ATPase Asna1	O54984	ARSA1_MOUSE	0.039747868
60	NSFL1 cofactor p47	Q9CZ44	NSF1C_MOUSE	0.027959581
61	Putative uncharacterized protein	Q3UWP8	Q3UWP8_MOUSE	0.027066861
62	Pyrroline-5-carboxylate reductase 3	Q9DCC4	P5CR3_MOUSE	0.023444497
63	Casein kinase I isoform alpha	Q8BK63	KC1A_MOUSE	0.022559068
64	Transketolase	P40142	TKT_MOUSE	0.009531475

Peroxiredoxin family proteins are highlighted by red. The glutathione system is highlighted by blue. The proteins catalizing NAD (P) $^{+}$ to NAD (P) H are highlighted by yellow.

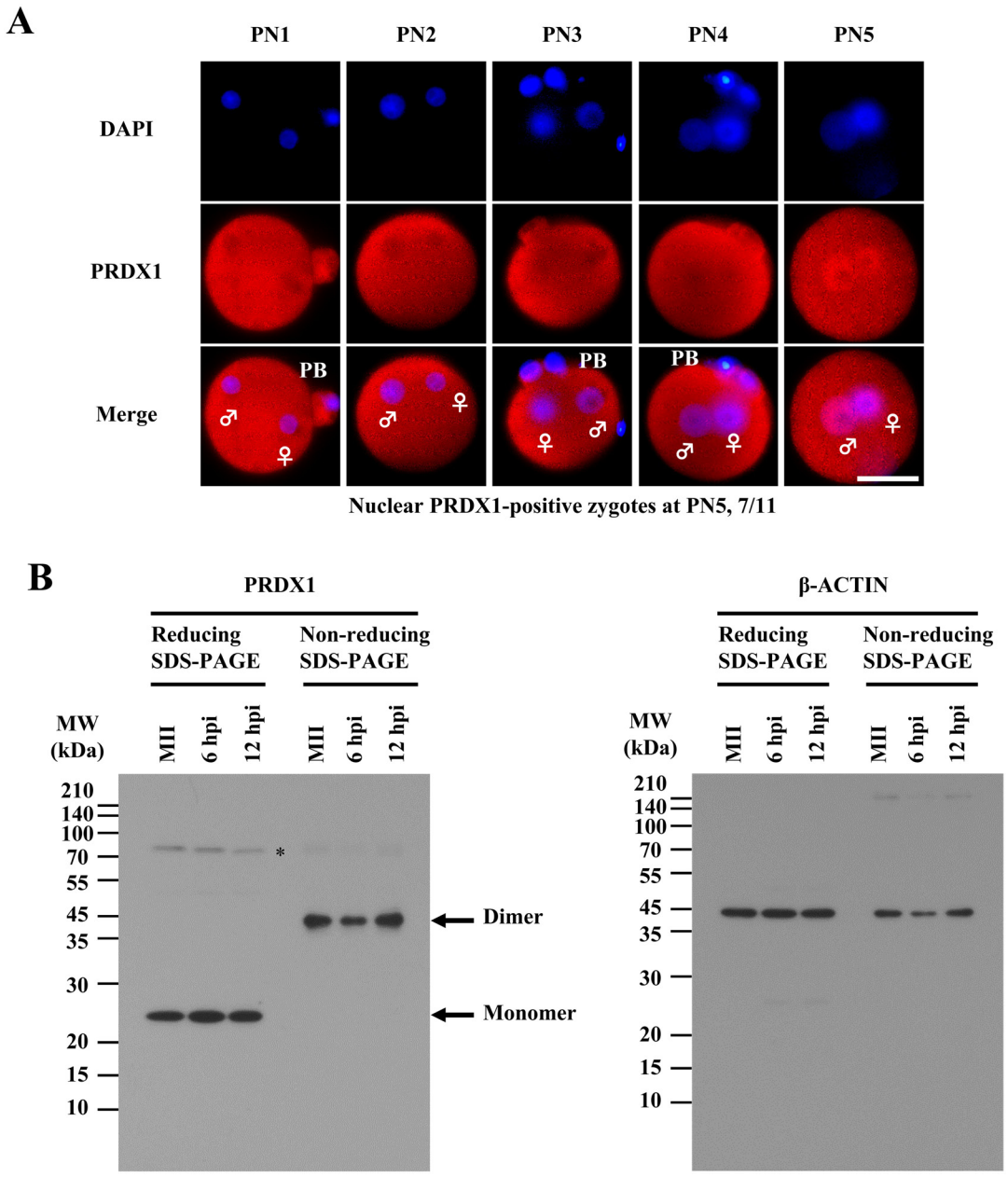

Fig. 2. Localization of PRDX1 and the existence of oxidized PRDX1 in zygotes at pronuclear stages. (A) Immunostaining for localization of PRDX1 at pronuclear stages (PN) 1–5. Shown are representative images of zygotes stained with DAPI (blue) and anti-PRDX1 antibody (red). Key: ♂, male pronucleus; ♀, female pronucleus; PB, polar body; scale bars = 50 μm. (B) Reduced and non-reduced immunoblots for PRDX1 at pronuclear stages. The bands predicted as nonspecific signal or covalent complexes are indicated by *. β-ACTIN was used as a loading control in immunoblot analyses. MW, molecular weight.

included in the 100 most abundant proteins in those tissues [42]. In particular, PRDX1 is included in the 100 most abundant proteins in 20 of these tissues [42]. On the other hand, PRDX2 is included in the 100 most abundant proteins in only 2 tissues, and the proteins of GSH system that directly eliminate H_2O_2, such as GPX, are not included in the 100 most abundant proteins in any tissues, while 7 types of GST are included in the 100 most abundant from 1-9 tissues [42]. In addition, SOD1 or SOD2 are included in the 100 most abundant proteins in 19 tissues [42]. According to another proteomics analysis using zygotes, SOD1 is indicated as the most abundant antioxidant in the identified proteins [43]. However, regarding the antioxidant enzymes involved in eliminating H_2O_2, PRDX1 is the most abundant antioxidant [43], which is in good agreement with our data. Thus, our results and these previous reports strongly

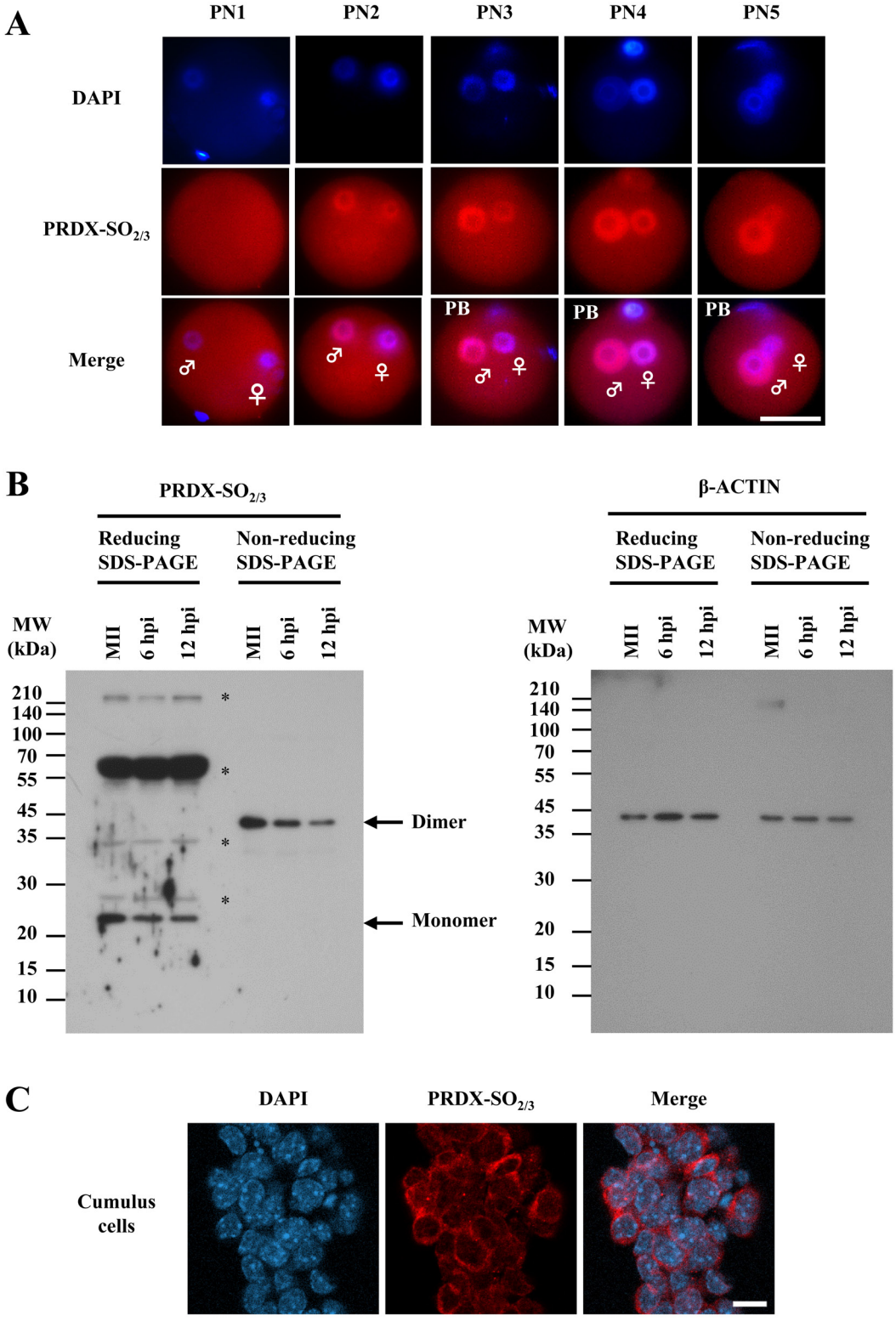

Fig. 3. Localization of PRDX-$SO_{2/3}$ in zygotes and somatic cells. (A) Immunostaining for localization of PRDX-$SO_{2/3}$ at pronuclear stages (PN) 1–5. Shown are representative images of zygotes stained with DAPI (blue) and anti-PRDX-$SO_{2/3}$ antibody (red). Key: ♂, male pronucleus; ♀, female pronucleus; PB, polar body; scale bars = 50 µm. (B) Reduced and non-reduced immunoblots for PRDX-$SO_{2/3}$ at pronuclear stages. The bands predicted as nonspecific signal or covalent complexes are indicated by *. β-ACTIN was used as a loading control in immunoblot analyses. MW, molecular weight. (C) Immunostaining for localization of PRDX-$SO_{2/3}$ in cumulus cells. Shown are representative images of cumulus cells stained with DAPI (blue) and anti-PRDX-$SO_{2/3}$ antibody (red). Scale bars = 10 µm.

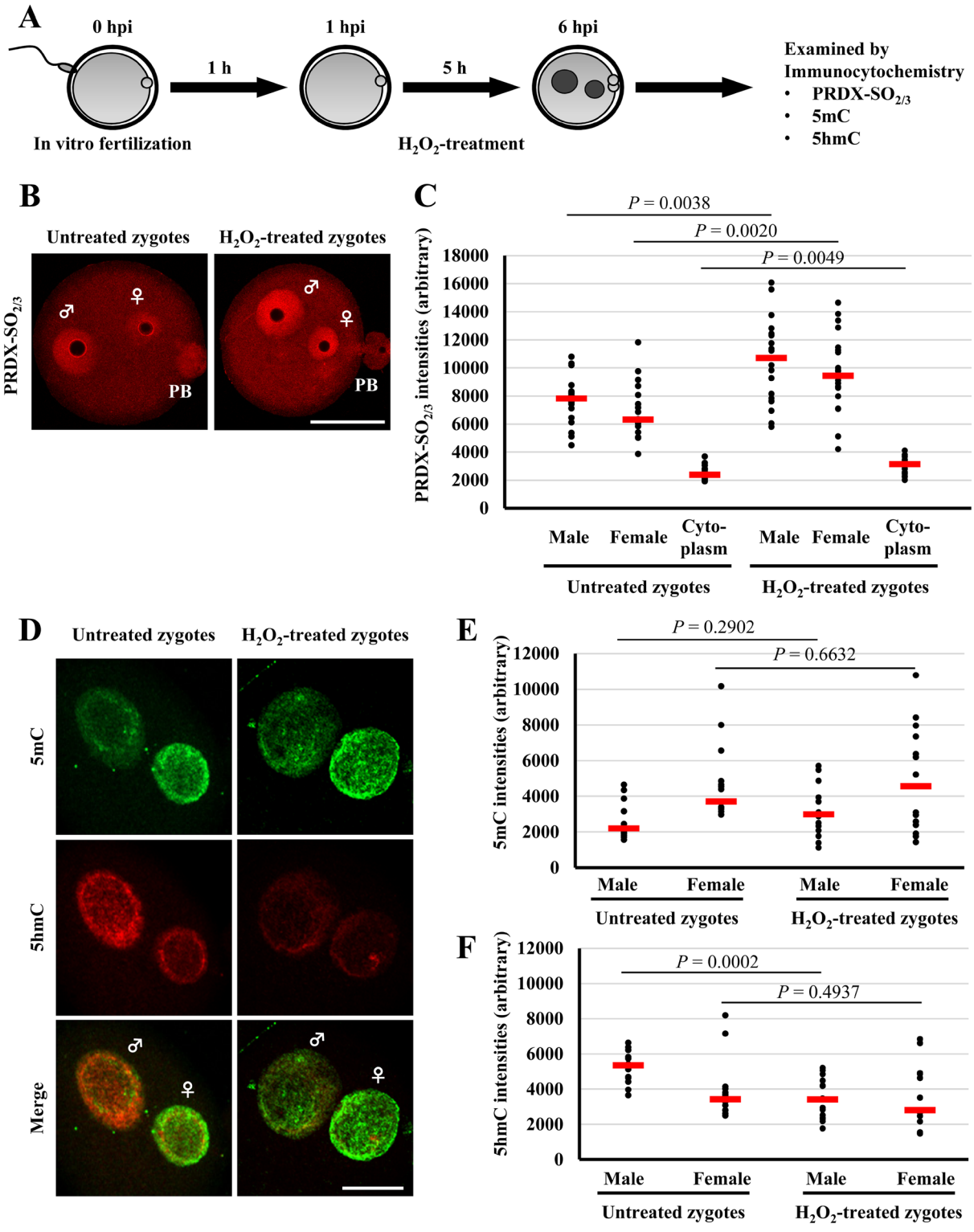

Fig. 4. Hyperoxidation of PRDX and accumulation of 5hmC on the male genome induced by H_2O_2-treatment. (A) Schematic diagram of the experimental procedure. (B) Immunostaining images of PRDX-$SO_{2/3}$ in untreated and H_2O_2-treated zygotes. Key: ♂, male pronucleus; ♀, female pronucleus. PB, polar body; scale bar = 50 µm. (C) Quantification of the ratio of PRDX-$SO_{2/3}$ intensities in untreated and H_2O_2-treated zygotes at 6 hpi. Red bars indicate the median values. The number of zygotes is 20 for each group. (D) Immunostaining images of 5mC (green) and 5hmC (red) in untreated and H_2O_2-treated zygotes. Key: ♂, male pronucleus; ♀, female pronucleus. Scale bar = 20 µm. (E) and (F) Quantification of the ratio of 5mC and 5hmC intensities in the pronucleus of untreated and H_2O_2-treated zygotes at 6 hpi. Red bars indicate the median values. The number of zygotes is 15 for each group.

support that PRDX1 is abundantly expressed as an antioxidant enzyme eliminating H_2O_2 in a wide range of cells, including MII oocytes and zygotes. PRDX1 and SOD1 may mainly play a role in eliminating H_2O_2 and superoxide, respectively, in various cells. Not only PRDX1 and PRDX2 identified by our investigation but also all isoforms of the PRDX family (PRDX1-6) in MII oocytes and zygotes are identified in the previous report [43]. Furthermore, another proteomics analysis indicates that PRDX2 and PRDX4 are highly expressed proteins in porcine fibroblast cell nuclei incubated in extracts from MII oocytes, as compared with those in germinal vesicle (GV) oocytes or fibroblast cells [44]. Taken together, PRDX family members might be actively involved in eliminating H_2O_2 in fertilized oocytes and early embryos as well as somatic cells.

As shown in Fig. 3A and 3C, our results suggest the possibility of specific functions for of PRDX family members as endogenous antioxidant enzymes in pronuclei of zygotes. In the previous reports, as for the antioxidant enzyme in nuclei of cells, nucleoredoxin (NRX) has been discovered by its overexpression [45, 46]. In fact, it has been reported that endogenous NRX exists predominantly in the cytoplasm of cultured cells by cell fractionation [47]. While the endogenous antioxidant enzymes actively existing in the nucleus has been uncertain, our data provide the first evidence that PRDX1 and other PRDX family members are pronuclear-localized antioxidant enzymes in zygotes. The pronuclear PRDX1 signals were observed at PN5 compared to other stages while PRDX1 functions before fertilization (Fig. 2B). PN5 (largely during 10–12 hpi) zygotes are mostly in G2 phase [31, 33], and according to the previous report, the H_2O_2-treated zygotes in G1 phase (at 7 hpi) are shown to significantly delay their entry to G2/M phase and to decrease the ratio of embryos that develop to the 2-cell stage [48, 49]. Thus, not to delay G2/M checkpoint activation induced by H_2O_2 as much as possible, PRDX1 might play a role in eliminating H_2O_2 in the pronucleus with the other PRDX family for normal embryo development. However, *Prdx1* knockout mice are viable, although they have a shortened lifespan due to the development of severe haemolytic anemia and several malignant cancers beginning at about 9 months of age, and the DNA damage is significantly elevated in some murine tissues [50, 51]. In addition, *Prdx2* knockout mice have been reported to show similar phenotypes [52]. Thus, some PRDX proteins might compensate for eliminating H_2O_2 even though one kind of *Prdx* is lacking in an early embryonic development. While pronuclear PRDX1 was observed at a later pronuclear stage, hyperoxidized PRDX signals were observed in pronuclei from PN2 (Fig. 2A and 3A). The other report shows that PRDX2 is not observed in pronuclei at PN3 [53]. Therefore, pronuclear hyperoxidized PRDX proteins around PN3 may be any of PRDX3-6. On the other hand, we could not observe any hyperoxidized PRDX signals in the nuclei of cumulus cells despite their exposure to the same stress environment as the zygotes (Fig. 3C). Therefore, PRDX proteins appear to specifically function as endogenous antioxidant enzymes in pronuclei of zygotes.

We also observed that treatment of zygotes at the pronuclear stage with H_2O_2 impaired the generation of 5hmC on the male genome but showed no significant effect on the existing 5mC (Fig. 4D, 4E, 4F, and Supplementary Fig. 1B). Since spermatic 5mC is removed independently of Tet3, and then *de novo* 5mC by DNA methyltransferases (DNMTs) is converted to 5hmC by Tet3 in zygotes [54], we speculate that the activity of Tet3 and DNMTs might be depressed under the oxidative stress induced by the H_2O_2-treatment. Indeed, H_2O_2 exposure results in lowered Tet3 activity in cultured mammalian cells [55]. As mentioned above, we found that PRDX proteins appear to specifically function as endogenous antioxidant enzymes in the pronuclei of zygotes. Taken together, our results suggest that epigenetic reprogramming might be regulated under ROS conditions moderated by PRDX-mediated antioxidant mechanisms during the maternal-to-zygotic transition (MZT). Correspondingly, the observation that preventing oxidative stress is important for epigenetic reprogramming, is shown in a recent report, in which treatment with the antioxidant, vitamin C after exposure to the HDAC inhibitor, trichostatin A, dramatically improves cloning efficiency in somatic cell nuclear transfer (SCNT) embryos [56]. Further studies are needed to elucidate how PRDX-mediated antioxidant mechanisms are involved in epigenetic reprogramming during MZT.

Acknowledgements

We thank Ms N Backes-Kamimura and Mr J Horvat for English editing.

This study was supported, in part, by JSPS KAKENHI Grant Number JP25292189 (to KMa), a grant from the INAMORI Foundation (to KMa), the Human Frontier Science Program (RGP0021/2016) (to KMi), JSPS KAKENHI Grant Numbers JP16H01321, JP16H01222 and JP17H05045 (to KMi), and a Grant for Basic Science Research Projects from The Sumitomo Foundation (150810) (to KMi).

References

1. **Tiwari M, Prasad S, Tripathi A, Pandey AN, Singh AK, Shrivastav TG, Chaube SK.** Involvement of reactive oxygen species in meiotic cell cycle regulation and apoptosis in mammalian oocytes. *Reactive Oxygen Species* 2016; **1**: 110–116. [CrossRef]
2. **Ray PD, Huang BW, Tsuji Y.** Reactive oxygen species (ROS) homeostasis and redox regulation in cellular signaling. *Cell Signal* 2012; **24**: 981–990. [Medline] [CrossRef]
3. **Reczek CR, Chandel NS.** ROS-dependent signal transduction. *Curr Opin Cell Biol* 2015; **33**: 8–13. [Medline] [CrossRef]
4. **Guérin P, El Mouatassim S, Ménézo Y.** Oxidative stress and protection against reactive oxygen species in the pre-implantation embryo and its surroundings. *Hum Reprod Update* 2001; **7**: 175–189. [Medline] [CrossRef]
5. **Takahashi M.** Oxidative stress and redox regulation on in vitro development of mammalian embryos. *J Reprod Dev* 2012; **58**: 1–9. [Medline] [CrossRef]
6. **Drevet JR.** The antioxidant glutathione peroxidase family and spermatozoa: a complex story. *Mol Cell Endocrinol* 2006; **250**: 70–79. [Medline] [CrossRef]
7. **Tsunoda S, Kawano N, Miyado K, Kimura N, Fujii J.** Impaired fertilizing ability of superoxide dismutase 1-deficient mouse sperm during in vitro fertilization. *Biol Reprod* 2012; **87**: 121. [Medline] [CrossRef]
8. **Wu G, Fang YZ, Yang S, Lupton JR, Turner ND.** Glutathione metabolism and its implications for health. *J Nutr* 2004; **134**: 489–492. [Medline] [CrossRef]
9. **Shi ZZ, Osei-Frimpong J, Kala G, Kala SV, Barrios RJ, Habib GM, Lukin DJ, Danney CM, Matzuk MM, Lieberman MW.** Glutathione synthesis is essential for mouse development but not for cell growth in culture. *Proc Natl Acad Sci USA* 2000; **97**: 5101–5106. [Medline] [CrossRef]
10. **Lu J, Holmgren A.** The thioredoxin antioxidant system. *Free Radic Biol Med* 2014; **66**: 75–87. [Medline] [CrossRef]
11. **Matsui M, Oshima M, Oshima H, Takaku K, Maruyama T, Yodoi J, Taketo MM.** Early embryonic lethality caused by targeted disruption of the mouse thioredoxin gene. *Dev Biol* 1996; **178**: 179–185. [Medline] [CrossRef]
12. **Nasr-Esfahani MM, Johnson MH.** The origin of reactive oxygen species in mouse embryos cultured in vitro. *Development* 1991; **113**: 551–560. [Medline]
13. **Lopes AS, Lane M, Thompson JG.** Oxygen consumption and ROS production are increased at the time of fertilization and cell cleavage in bovine zygotes. *Hum Reprod*

2010; **25**: 2762–2773. [Medline] [CrossRef]
14. **McLay DW, Clarke HJ.** Remodelling the paternal chromatin at fertilization in mammals. *Reproduction* 2003; **125**: 625–633. [Medline] [CrossRef]
15. **Tosti E, Ménézo Y.** Gamete activation: basic knowledge and clinical applications. *Hum Reprod Update* 2016; **22**: 420–439. [Medline] [CrossRef]
16. **Takahashi M, Saka N, Takahashi H, Kanai Y, Schultz RM, Okano A.** Assessment of DNA damage in individual hamster embryos by comet assay. *Mol Reprod Dev* 1999; **54**: 1–7. [Medline] [CrossRef]
17. **Liu L, Trimarchi JR, Keefe DL.** Involvement of mitochondria in oxidative stress-induced cell death in mouse zygotes. *Biol Reprod* 2000; **62**: 1745–1753. [Medline] [CrossRef]
18. **Pirson M, Knoops B.** Expression of peroxiredoxins and thioredoxins in the mouse spinal cord during embryonic development. *J Comp Neurol* 2015; **523**: 2599–2617. [Medline] [CrossRef]
19. **Mizuno S, Sono Y, Matsuoka T, Matsumoto K, Saeki K, Hosoi Y, Fukuda A, Morimoto Y, Iritani A.** Expression and subcellular localization of GSE protein in germ cells and preimplantation embryos. *J Reprod Dev* 2006; **52**: 429–438. [Medline] [CrossRef]
20. **Matsuoka T, Sato M, Tokoro M, Shin SW, Uenoyama A, Ito K, Hitomi S, Amano T, Anzai M, Kato H, Mitani T, Saeki K, Hosoi Y, Iritani A, Matsumoto K.** Identification of ZAG1, a novel protein expressed in mouse preimplantation, and its putative roles in zygotic genome activation. *J Reprod Dev* 2008; **54**: 192–197. [Medline] [CrossRef]
21. **Shin SW, Tokoro M, Nishikawa S, Lee HH, Hatanaka Y, Nishihara T, Amano T, Anzai M, Kato H, Mitani T, Kishigami S, Saeki K, Hosoi Y, Iritani A, Matsumoto K.** Inhibition of the ubiquitin-proteasome system leads to delay of the onset of ZGA gene expression. *J Reprod Dev* 2010; **56**: 655–663. [Medline] [CrossRef]
22. **Tokoro M, Shin SW, Nishikawa S, Lee HH, Hatanaka Y, Amano T, Mitani T, Kato H, Anzai M, Kishigami S, Saeki K, Hosoi Y, Iritani A, Matsumoto K.** Deposition of acetylated histones by RNAP II promoter clearance may occur at onset of zygotic gene activation in preimplantation mouse embryos. *J Reprod Dev* 2010; **56**: 607–615. [Medline] [CrossRef]
23. **Shin SW, Shimizu N, Tokoro M, Nishikawa S, Hatanaka Y, Anzai M, Hamazaki J, Kishigami S, Saeki K, Hosoi Y, Iritani A, Murata S, Matsumoto K.** Mouse zygote-specific proteasome assembly chaperone important for maternal-to-zygotic transition. *Biol Open* 2013; **2**: 170–182. [Medline] [CrossRef]
24. **Hatanaka Y, Shimizu N, Nishikawa S, Tokoro M, Shin SW, Nishihara T, Amano T, Anzai M, Kato H, Mitani T, Hosoi Y, Kishigami S, Matsumoto K.** GSE is a maternal factor involved in active DNA demethylation in zygotes. *PLoS ONE* 2013; **8**: e60205. [Medline] [CrossRef]
25. **Nishikawa S, Hatanaka Y, Tokoro M, Shin SW, Shimizu N, Nishihara T, Kato R, Takemoto A, Amano T, Anzai M, Kishigami S, Hosoi Y, Matsumoto K.** Functional analysis of nocturnin, a circadian deadenylase, at maternal-to-zygotic transition in mice. *J Reprod Dev* 2013; **59**: 258–265. [Medline] [CrossRef]
26. **Lawitts JA, Biggers JD.** Culture of preimplantation embryos. *Methods Enzymol* 1993; **225**: 153–164. [Medline] [CrossRef]
27. **Nagai K, Yotsukura N, Ikegami H, Kimura H, Morimoto K.** Protein extraction for 2-DE from the lamina of Ecklonia kurome (laminariales): recalcitrant tissue containing high levels of viscous polysaccharides. *Electrophoresis* 2008; **29**: 672–681. [Medline] [CrossRef]
28. **Satoh M, Tokoro M, Ikegami H, Nagai K, Sono Y, Shin SW, Nishikawa S, Saeki K, Hosoi Y, Iritani A, Fukuda A, Morimoto Y, Matsumoto K.** Proteomic analysis of the mouse ovary in response to two gonadotropins, follicle-stimulating hormone and luteinizing hormone. *J Reprod Dev* 2009; **55**: 316–326. [Medline] [CrossRef]
29. **Shimizu N, Ueno K, Kurita E, Shin SW, Nishihara T, Amano T, Anzai M, Kishigami S, Kato H, Mitani T, Hosoi Y, Matsumoto K.** Possible role of ZPAC, zygote-specific proteasome assembly chaperone, during spermatogenesis in the mouse. *J Reprod Dev* 2014; **60**: 179–186. [Medline] [CrossRef]
30. **Schröder E, Brennan JP, Eaton P.** Cardiac peroxiredoxins undergo complex modifications during cardiac oxidant stress. *Am J Physiol Heart Circ Physiol* 2008; **295**: H425–H433. [Medline] [CrossRef]
31. **Santos F, Hendrich B, Reik W, Dean W.** Dynamic reprogramming of DNA methylation in the early mouse embryo. *Dev Biol* 2002; **241**: 172–182. [Medline] [CrossRef]
32. **Inoue A, Zhang Y.** Replication-dependent loss of 5-hydroxymethylcytosine in mouse preimplantation embryos. *Science* 2011; **334**: 194. [Medline] [CrossRef]
33. **Adenot PG, Mercier Y, Renard JP, Thompson EM.** Differential H4 acetylation of paternal and maternal chromatin precedes DNA replication and differential transcriptional activity in pronuclei of 1-cell mouse embryos. *Development* 1997; **124**: 4615–4625. [Medline]
34. **Matsumoto K, Anzai M, Nakagata N, Takahashi A, Takahashi Y, Miyata K.** Onset of paternal gene activation in early mouse embryos fertilized with transgenic mouse sperm. *Mol Reprod Dev* 1994; **39**: 136–140. [Medline] [CrossRef]
35. **Rhee SG, Kang SW, Chang TS, Jeong W, Kim K.** Peroxiredoxin, a novel family of peroxidases. *IUBMB Life* 2001; **52**: 35–41. [Medline] [CrossRef]
36. **Rhee SG, Chae HZ, Kim K.** Peroxiredoxins: a historical overview and speculative preview of novel mechanisms and emerging concepts in cell signaling. *Free Radic Biol Med* 2005; **38**: 1543–1552. [Medline] [CrossRef]
37. **Neumann CA, Cao J, Manevich Y.** Peroxiredoxin 1 and its role in cell signaling. *Cell Cycle* 2009; **8**: 4072–4078. [Medline] [CrossRef]
38. **Rhee SG, Woo HA, Kil IS, Bae SH.** Peroxiredoxin functions as a peroxidase and a regulator and sensor of local peroxides. *J Biol Chem* 2012; **287**: 4403–4410. [Medline] [CrossRef]
39. **ONeill JS, Reddy AB.** Circadian clocks in human red blood cells. *Nature* 2011; **469**: 498–503. [Medline] [CrossRef]
40. **Gu TP, Guo F, Yang H, Wu HP, Xu GF, Liu W, Xie ZG, Shi L, He X, Jin SG, Iqbal K, Shi YG, Deng Z, Szabó PE, Pfeifer GP, Li J, Xu GL.** The role of Tet3 DNA dioxygenase in epigenetic reprogramming by oocytes. *Nature* 2011; **477**: 606–610. [Medline] [CrossRef]
41. **Wossidlo M, Nakamura T, Lepikhov K, Marques CJ, Zakhartchenko V, Boiani M, Arand J, Nakano T, Reik W, Walter J.** 5-Hydroxymethylcytosine in the mammalian zygote is linked with epigenetic reprogramming. *Nat Commun* 2011; **2**: 241. [Medline] [CrossRef]
42. **Geiger T, Velic A, Macek B, Lundberg E, Kampf C, Nagaraj N, Uhlen M, Cox J, Mann M.** Initial quantitative proteomic map of 28 mouse tissues using the SILAC mouse. *Mol Cell Proteomics* 2013; **12**: 1709–1722. [Medline] [CrossRef]
43. **Wang S, Kou Z, Jing Z, Zhang Y, Guo X, Dong M, Wilmut I, Gao S.** Proteome of mouse oocytes at different developmental stages. *Proc Natl Acad Sci USA* 2010; **107**: 17639–17644. [Medline] [CrossRef]
44. **Miyamoto K, Nagai K, Kitamura N, Nishikawa T, Ikegami H, Binh NT, Tsukamoto S, Matsumoto M, Tsukiyama T, Minami N, Yamada M, Ariga H, Miyake M, Kawarasaki T, Matsumoto K, Imai H.** Identification and characterization of an oocyte factor required for development of porcine nuclear transfer embryos. *Proc Natl Acad Sci USA* 2011; **108**: 7040–7045. [Medline] [CrossRef]
45. **Kurooka H, Kato K, Minoguchi S, Takahashi Y, Ikeda J, Habu S, Osawa N, Buchberg AM, Moriwaki K, Shisa H, Honjo T.** Cloning and characterization of the nucleoredoxin gene that encodes a novel nuclear protein related to thioredoxin. *Genomics* 1997; **39**: 331–339. [Medline] [CrossRef]
46. **Hirota K, Matsui M, Murata M, Takashima Y, Cheng FS, Itoh T, Fukuda K, Yodoi J.** Nucleoredoxin, glutaredoxin, and thioredoxin differentially regulate NF-kappaB, AP-1, and CREB activation in HEK293 cells. *Biochem Biophys Res Commun* 2000; **274**: 177–182. [Medline] [CrossRef]
47. **Funato Y, Michiue T, Asashima M, Miki H.** The thioredoxin-related redox-regulating protein nucleoredoxin inhibits Wnt-β-catenin signalling through dishevelled. *Nat Cell Biol* 2006; **8**: 501–508. [Medline] [CrossRef]
48. **Qian D, Li Z, Zhang Y, Huang Y, Wu Q, Ru G, Chen M, Wang B.** Response of mouse zygotes treated with mild hydrogen peroxide as a model to reveal novel mechanisms of oxidative stress-induced injury in early embryos. *Oxid Med Cell Longev* 2016; **2016**: 1521428. [Medline] [CrossRef]
49. **Zhang Y, Qian D, Li Z, Huang Y, Wu Q, Ru G, Chen M, Wang B.** Oxidative stress-induced DNA damage of mouse zygotes triggers G2/M checkpoint and phosphorylates Cdc25 and Cdc2. *Cell Stress Chaperones* 2016; **21**: 687–696. [Medline] [CrossRef]
50. **Neumann CA, Krause DS, Carman CV, Das S, Dubey DP, Abraham JL, Bronson RT, Fujiwara Y, Orkin SH, Van Etten RA.** Essential role for the peroxiredoxin Prdx1 in erythrocyte antioxidant defence and tumour suppression. *Nature* 2003; **424**: 561–565. [Medline] [CrossRef]
51. **Egler RA, Fernandes E, Rothermund K, Sereika S, de Souza-Pinto N, Jaruga P, Dizdaroglu M, Prochownik EV.** Regulation of reactive oxygen species, DNA damage, and c-Myc function by peroxiredoxin 1. *Oncogene* 2005; **24**: 8038–8050. [Medline] [CrossRef]
52. **Lee TH, Kim SU, Yu SL, Kim SH, Park DS, Moon HB, Dho SH, Kwon KS, Kwon HJ, Han YH, Jeong S, Kang SW, Shin HS, Lee KK, Rhee SG, Yu DY.** Peroxiredoxin II is essential for sustaining life span of erythrocytes in mice. *Blood* 2003; **101**: 5033–5038. [Medline] [CrossRef]
53. **Wang S, Huang W, Shi H, Lin C, Xie M, Wang J.** Localization and expression of peroxiredoxin II in the mouse ovary, oviduct, uterus, and preimplantation embryo. *Anat Rec (Hoboken)* 2010; **293**: 291–297. [Medline] [CrossRef]
54. **Amouroux R, Nashun B, Shirane K, Nakagawa S, Hill PW, DSouza Z, Nakayama M, Matsuda M, Turp A, Ndjetehe E, Encheva V, Kudo NR, Koseki H, Sasaki H, Hajkova P.** De novo DNA methylation drives 5hmC accumulation in mouse zygotes. *Nat Cell Biol* 2016; **18**: 225–233. [Medline] [CrossRef]
55. **Niu Y, DesMarais TL, Tong Z, Yao Y, Costa M.** Oxidative stress alters global histone modification and DNA methylation. *Free Radic Biol Med* 2015; **82**: 22–28. [Medline] [CrossRef]
56. **Miyamoto K, Tajima Y, Yoshida K, Oikawa M, Azuma R, Allen GE, Tsujikawa T, Tsukaguchi T, Bradshaw CR, Jullien J, Yamagata K, Matsumoto K, Anzai M, Imai H, Gurdon JB, Yamada M.** Reprogramming towards totipotency is greatly facilitated by synergistic effects of small molecules. *Biol Open* 2017; **6**: 415–424. [Medline] [CrossRef]